Postprint of: Husev O., Vinnikov D., Roncero-Clemente C., Blaabjerg F., Strzelecki R., MPPT and GMPPT Implementation for Buck-Boost Mode Control of quasi-Z-Source Inverter, IEEE TRANSACTIONS ON INDUSTRIAL ELECTRONICS (2021), DOI: 10.1109/TIE.2021.3125658

MPPT and GMPPT Implementation for Buck-Boost Mode Control of quasi-Z-Source Inverter

Oleksandr Husev, *Senior Member, IEEE*, Dmitri Vinnikov, *Senior Member, IEEE*, Carlos Roncero-Clemente, *Senior Member, IEEE*, Frede Blaabjerg, *Fellow, IEEE*, Ryszard Strzelecki, *Member, IEEE*

***Abstract*—The focus is on the maximum power point tracking implementation for the buck-boost voltage mode control of a single-phase multilevel inverter based on a three-level neutral point clamped quasi-Z-source topology. To utilize shoot-through states only when boost function is needed and avoid it in the buck mode, two different control approaches are required. This work proposes merged control system which provides switching between different control algorithms in the buck and boost modes. In particular, a hysteresis band between the buck and boost modes is proposed which provides smooth and stable performance. It also includes features of the implementation of the global maximum power point tracking, which can scan the entire input voltage range in up to 10 seconds. Experimental results showed that proposed control system provides high and stable MPPT efficiency in different operation points. Finally, the key features are verified, the advantages, drawbacks, and an eventual potential for other applications are presented in conclusions.**

***Index Terms*— Quasi-Z-source Inverter; Multilevel Inverter; Photovoltaic Systems; Maximum Power Point Tracking.**

I. Introduction

Z-Source (ZS) and quasi-Z-Source (qZS) inverters have been proposed in [1], [2]. They allow overcoming some typical limitations associated with the conventional voltage-source inverters: both have buck and boost operation modes and they are not affected by Shoot-Through (ST) switching states, which correspond to a short-circuit condition in one or more inverter phase-legs. In advance, qZS inverters are suitable for drawing a Continuous Input Current (CIC) from the power source and for sharing a common ground-point with the dc-source. These benefits are suitable for renewable energy applications, in particular, for the Photovoltaic (PV) systems.

Over the years, ZS and qZS networks have been verified in several applications [3]-[5]. In [3], the application of the qZS network for the isolated dc-dc converter was demonstrated, while the application of wireless power transfer is exemplified in [4]. Among other efforts, an attempt to design a commercial prototype of a solar microinverter can be underlined [5].

Neutral-Point-Clamped (NPC) inverter is one of the most attractive solutions for industrial applications [6]. Among multilevel topologies, NPC became popular because of its low capacitor count. The qZSI was extended to the 3-Level (3L) and cascaded application as well [7]-[10]. The 3L-NPC qZSI topology (Fig. 1) was considered because of its traditional advantages, including the output power quality, ST immunity and power range. In addition, it has a very wide input voltage range, which is suitable for PV applications. PV systems provide a variable output voltage due to different irradiance and temperature levels; as a result, buck and boost modes are required.

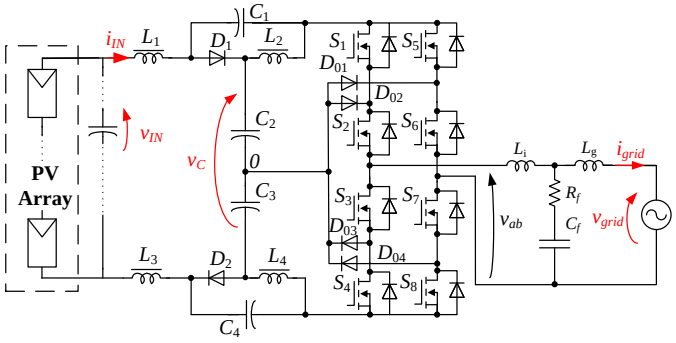

Fig. 1. Single-phase 3L-NPC qZS-based PV grid-connected system [8].

The solution presented in Fig. 1 was first described and experimentally verified in [7] in the open loop mode. Some disadvantages reported in [11], [12]. On the other hand, it was finalized as a pre-industrial solar inverter prototype [13]. It was concluded that this solution has reduced common mode voltage

Manuscript received July 1, 2021; revised September 28, 2021; accepted October 25, 2021. This work was supported in part by the by the Estonian Research Council grant PRG1086 and by the Estonian Centre of Excellence in Zero Energy and Resource Efficient Smart Buildings and Districts (ZEBE).

O. Husev and D. Vinnikov are with the Tallinn University of Technology, Tallinn, 19086, Ehitajate tee 5, Estonia (e-mail: oleksandr.husev@taltech.ee, dmitri.vinnikov@taltech.ee).

C. Roncero-Clemente and E. Romero-Cadaval are with Extremadura University, Badajoz, Spain. (e-mail: croncero@peandes.net).

Frede Blaabjerg is with the Institute of Energy Technology, Aalborg University, Pontoppidanstræde, str. 101, 9220 Aalborg, Denmark (email: fbl@et.aau.dk).

R. Strzelecki is with the Gdansk University of Technology, Gdańsk, Gabriela Narutowicza 11/12, 80-233 Poland (email: ryszard.strzelecki@pg.edu.pl).

and EMI filters correspondingly. The real advantage of ST immunity consists in the simplification of driver circuits of power switches. The inverter does not suffer from the short-circuit problem, i.e., only unipolar gate drivers can be used.

The main goal of this research work is to design an efficient Maximum Power Point Tracking (MPPT) for the qZS-based solar inverter, which will combine the buck-boost control capability and the grid-connection algorithm. Moreover, Global MPPT (GMPPT) is considered as a particular case of MPPT. The MPPT efficiency is the main criterion of the control system effectiveness.

Many studies focus on the MPPT performance of the qZS-based inverters [14]-[23]. The results of in-depth analyses of the existing methods have showed that they lack several practical issues that concern differences between the buck and boost modes along with MPPT. No studies in the reviewed research literature demonstrate features of the Global MPPT (GMPPT) implementation for the qZS-based string solar inverters [24].

The paper is organized as follows. Section II reviews the state-of-the-art of the existing MPPT approaches for the qZS inverters. Section III summarized passive components design guidelines. The next section IV describes in detail the proposed control system. Section V focuses on the hysteresis band between the buck and boost modes. Features of the MPPT and GMPPT implementation are addressed in Section VI. Finally, results from the evaluation of an experimental prototype are presented in Section VII. The main advantages and recommendations are covered in conclusions.

II. Existing MPPT Approaches for qZS Inverters

Several different PV profiles that can be configured for solar string inverter are depicted in Fig. 2*a*. For example, the PV array can be composed in order to make Standard Test Conditions (STC) gives MPP voltage more than 400 V, which corresponds to the buck mode of the converter (curve A). The partial shading case is shown separately in Fig. 2*b*. Shading of 3 out of 12 panels gives 2 local maximum points (point MPP1 and MPP2). It is evident that in the case of a classical MPPT algorithm, the solar inverter will stuck in point MPP1, which may give only 30% of energy available from the PV string. Different cases of partial shading condition can be observed in other works [25], [26].

The boost mode is required for the second case (curve B). It corresponds to the example with reduced number of installed panels compare to the curve A.

Finally, the third case (curve C) corresponds to the 360 V MPP which is derived from profile A in case of lower solar irradiance (cloudy weather, fog etc.). It is close to the boundary between the buck and boost operation modes of the inverter.

Fig. 2 demonstrates that any solar inverter based on the ZS or qZS network has to be able to work in the buck and boost modes with corresponding MPPT algorithms. The GMMP algorithm that may help working in the optimal point has to be available as well. Most of the different MPPT approaches discussed in the research literature for qZS-based solar inverters can be classified based on the output signal of the MPPT block.

First of all, works [10], [16]-[20] describe the MPPT performance of the qZS inverter based on the implementation of the ST states. They pay attention to the details such as the type of MPPT, fixed or variable step, etc. These studies do not consider the situation when the input voltage is higher than minimal required capacitor voltage and the ST states are not necessary and even dangerous due to the overboost performance. In any case, additional losses are introduced by ST states generation.

The second type of the MPPT approach is based on the reference grid current I_{grid}* or the reference grid power control and is not in a response for ST states implementation [7], [15]. The ST states are generated for power decoupling and average capacitor voltage control by other blocks. This approach is feasible for a very fast voltage control system. The main limitation concerns power balance between the input and the output.

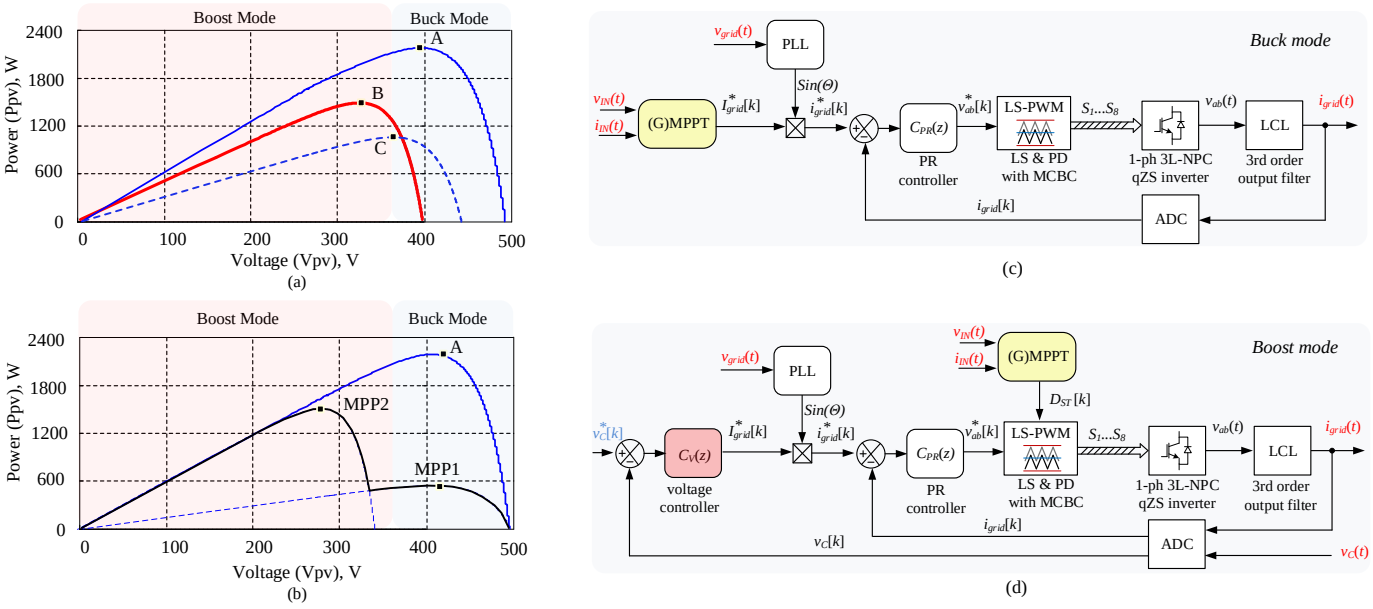

Fig. 2. Examples of the power-voltage curves of the different PV string arrays (a and b) along with proposed control system for buck (c) and boost mode (d) [13].

The MPPT block is the slowest algorithm in the system. As a result, during the MPPT performance, the reference grid power (current) can be significantly higher than available energy from the PV string. Large input capacitors such as energy buffers are a universal solution in order to improve the dynamic of the control system [27]. But the PV capacitor is minimized in this case and low frequency mitigation function is distributed between qZS network capacitors [13].

Some other non-conventional approaches can be considered. The studies in [21]-[23] have proposed completely different MPPT approaches based on the Model Predictive Control (MPC). It covers all operation modes but like any MPC, it may require significant computational resources, whereas some of them are not confirmed by experimental verification. In [22], only the boost mode is demonstrated.

As a conclusion, none of the above-mentioned papers consider a different control system for the buck and boost modes. Some works propose universal solutions, but they have computational or dynamic limitations. Also, it should be mentioned that only [20] considers the GMPPT implementation issue for the qZS-based converter, but it cannot be considered as a reference study for our case due to significant topological and functional differences.

III. PASSIVE COMPONENTS DESIGN SUMMARY

The main aim of the passive component's selection is to provide proper operation of a solar inverter. The values of components are interconnected with the switching frequency, which, in turn, is interconnected with the efficiency. The components can not be oversized due to the cost limitation.

Passive components of the qZS network are selected to mitigate the double-frequency power ripple along with high-switching frequency ripple, which is required in order to provide MPPT efficiency not less than 99 %. The so-called power decoupling approach is widely used in the single-phase systems [29], [30]. Passive elements of the qZS network have to be able to mitigate the double frequency power ripple in order to provide the PV panel's voltage ripple $\Delta V_{PV}/V_{PV}$ not higher than 3-4 %. This percentage is sufficient to provide the MPPT efficiency not lower than 99 %, which is the industrial standard [31]. At the same time, due to the qZS network structure, the input decoupling capacitors are not required. In this particular case, the input capacitor corresponds to the capacitance of PV panels and is not significant.

Taking into account the size and price optimization, it is necessary to calculate the minimal values of passive components that are able to provide the above-mentioned MPPT efficiency.

We assumed that, the voltage ripple K_{CL2} across qZS network capacitors is defined by low-frequency power ripple and the capacitors can be defined as following:

$$C \geq \frac{2 \cdot P_{IN} \cdot T}{\pi \cdot V_{C\_REF}^2 \cdot K_{CL2}}, \qquad (1)$$

where T is a period of the fundamental cycle, P_{IN} is input power, $<v_C>=v_{C\_REF}$ is an average voltage across internal capacitors C_2 and C_3 which defines the border between buck and boost mode. In a very general case the value of capacitors C_1 and C_4 can be equal to internal capacitors or smaller. The main conclusion is that the value of capacitors depends on the output power level and does not depend on the input voltage.

The inductors are selected for the high-frequency switching current ripple factor K_{LH1} limitation:

$$L \geq \frac{V_g^2 \cdot (V_{C\_REF} - V_{IN}) \cdot T_S \cdot V_{IN}}{2 \cdot K_{LH} \cdot P_{IN} \cdot V_{C\_REF} (2V_{C\_REF} - V_{IN})}, \qquad (2)$$

where T_S is a period of a switching cycle, V_{IN} – input voltage, V_g – RMS value of the grid voltage.

The selected components and main parameters are shown in Table I. This table also shows the parameters of the designed solar inverter that are typical for the industrial samples.

TABLE I.
SPECIFICATIONS OF THE CASE-STUDY QZS-BASED SOLAR INVERTER

Parameter	Value
Grid parameters	230 V, 50 Hz
Capacitors C_1 and C_4	2.70 mF
Capacitors C_2 and C_3	3.6 mF
Inductors L_1 - L_4	900 µH
1st filter inductance L_i (inverter) – LCL	440 µH
Filter capacitance C_f – LCL	15.47 µF
2nd filter inductance L_g (grid) – LCL	220 µH
Damping resistor R_f	0.8 Ohms
Switching frequency (MOSFET devices)	25-60 kHz
Sampling frequency	8 kHz
MPPT sampling frequency	5-10 Hz
MPPT, input voltage range	200 – 450V
Maximum input power	3.3 kW
Maximum input current	12 A
Input voltage range	150-600 V
THD of the grid current	<8 %

It can be seen that the relative current ripple depends on the power, switching frequency and the input voltage. Based on analysis conducted in [13] the variable switching frequency is applied in order to maximize overall efficiency of the converter.

Fig. 3 illustrates dependence of the switching frequency as function of input voltage and current, where ST duty cycle is expressed as following:

$$D_{ST} = \frac{(V_{C\_REF} - V_{IN})}{(2V_{C\_REF} - V_{IN})}. \qquad (3)$$

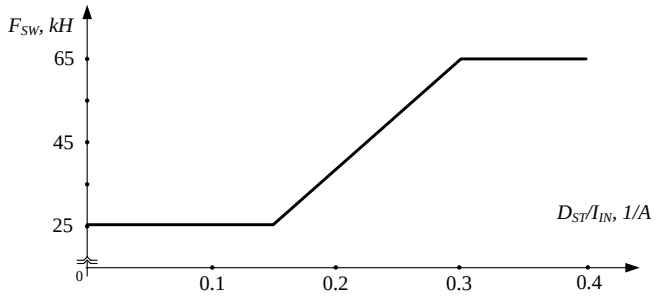

Fig. 3 switching frequency as a function of the ratio between ST duty cycle d_{ST} and average input current I_{IN}.

In the most operation points (when input current more than 2 A) the switching frequency has its minimal 25 kHz value. It helps to keep high efficiency, while the high level of the injected fundamental current keeps the relative input and output current ripples quite low. In case of power level reduction or significant boost requirement the switching frequency increasing (up to 65 kHz). It helps to reduce the input current ripple. It in turns helps to provide MPPT efficiency at stable and

high level along with avoiding problem with discontinuous conduction mode. Also, despite on switching frequency increasing, the overall efficiency can be even better due to the ripple and conduction losses reduction.

The output *LCL*-filter is calculated according to [28] in order to provide a THD value of the output current lower than 8 % for 75 % of the maximum output power. The cut-off frequency of the output filter has to be at least twice smaller compared to the sampling frequency.

IV. Control System Description

This section is devoted to the control system description. A general block diagram of the proposed control strategy for an internal capacitor voltage v_C (C_2 and C_3) regulation based on the buck-boost control is presented in Fig. 2. In this study, two possible control modes are considered: when the input voltage is below the reference value of the voltage v^*_C (boost mode) or higher (buck mode). This reference voltage across internal capacitors C_2 and C_3 has fixed and variable component:

$$v_C^* = V_{C\_REF} \pm \Delta v_C . \quad (4)$$

The variable component is defined by hysteresis band and is described in the next chapter. The fixed component V_{C_REF} is set to 380 V. This voltage can be decreased up to 340 V in the case of low power injection or very low grid impedance.

Both modes can be simply referred to by the term: the buck-boost control method. Two independent control systems are proposed correspondingly.

The first control system corresponds to the buck mode (Fig. 2*c*). In this mode, the MPPT is used for adjusting the reference grid current I^*_{grid} according to the operation point observed on the PV array. This mode is similar to the conventional operation of the Voltage Source Inverter (VSI), the qZS network is not utilized. Internal capacitors (C_2 and C_3) are controlled by the power balance while the voltage across other capacitors (C_1 and C_4) remains zero. The voltage v_{grid} corresponds to the voltage available at the PCC (point of common coupling) and the current i_{grid} corresponds to the amount of the ac current injected into the grid.

Fig. 2*d* shows the control system in the case of boost mode activation. The activation of this control loop happens when the input voltage drops below the threshold level. On the one hand, the current control loop remains the same. On the other hand, the voltage control loop is added. Closed-loop regulation of the capacitor voltage is performed by the controller $C_v(z)$, which provides the reference grid current I^*_{grid}. It provides balance of the energy flow between the PV array and the grid. The ST duty cycle is provided by the MPPT algorithm, which ensures necessary boost of the input voltage. This value is directly given to the modulation block. Capacitor voltage controller requires the dynamic model of the 3L NPC qZS-based inverter. A detailed analytical tuning approach is proposed in [32]. It is based on the ac small-signal modeling technique [33].

The ac reference grid current i^*_{grid} is elaborated by means of reference current I^*_{grid} multiplication with a sinusoidal signal from the Phase-Locked Loop (PLL) block. By the scalable factors, the waveform of the reference i^*_{grid} is synchronized with the fundamental component from the voltage at PCC (v_{grid}). Detailed tuning of the P+R controller is presented in [34], [35]. The current controller $C_{PR}(z)$ provides a reference voltage v^*_{ab} to be performed by the 3L-NPC qZS inverter in both modes. For that, all switching patterns of the inverter topology are defined by means of a modulation strategy called Level-Shift Modified PWM (LS-PWM) with Phase-Disposition (PD) of double carrier waveforms (5 levels). Details of the modulation strategy with the ST states are described in several research papers [7], [36]. The applied modulation strategy is also associated with the Maximum Constant Boost Control (MCBC) [36]. In difference to Maximum Boost Control (MBC) it does not evoke input current oscillation [37]. The modulation technique selected leads to an equal utilization of the capacitors C_2 and C_3, which, in turn, provides for the absence of the voltage disbalance across the capacitors. This goal can be achieved by Space Vector Pulse Width Modulation (SVPWM) technique that is more flexible, but requires more computational resources [38], [39].

The control system has to provide proper transients between the buck and boost modes. The GMPPT implementation requires additional analysis and has some specific features.

However, another approach could be also used in the boost mode. The reference grid current could be provided from the MPPT block, while the capacitor voltage could be regulated by the ST duty cycle. But the main problem lies in the stability of such approach. The MPPT block is the slowest control block in any solar inverter system and cannot be used in response to the reference grid current where the capacitor voltage regulation is required. The best performance in terms of stability and dynamic MPPT performance is achieved when the MPPT function is provided by ST duty cycle regulation; then, fast voltage control block defines the power balance between the PV system and the grid while the fastest control block is in response to the grid current control.

V. Hysteresis band Between Buck and Boost Modes

This section is devoted to the practical implementation of the buck and boost modes. The control system keeps the capacitor voltage under control. At the beginning of the MPPT routine, the input voltage is equal to the open circuit voltage of the PV string and the buck mode is activated. After that, voltage is descending, and the boost mode will be activated when the operating point passes the threshold value. In this way, the control system will keep capacitor voltage constant despite further input voltage decreasing.

Practical experience shows that appearance of even very small ST states will lead to the capacitor and input voltage disturbances. It means that the input voltage level higher than the threshold level can be detected. As a result, the control system may switch to the buck mode. It is evident that such approach will lead to the oscillation process between the buck and boost modes which, in turn, will lead to the deterioration of the solar inverter performance. To avoid that, the hysteresis band between the buck and boost modes is introduced. Fig. 4 illustrates the proposed approach. At the very beginning, the low irradiance level is considered. The open circuit voltage of the PV string can be about 400 V. The inverter starts working in the buck mode and the input voltage along with the capacitor voltage is decreasing until lower threshold is achieved. Due to

the hysteresis band, the lower threshold reference capacitor voltage is set to 370 V. After that, the boost mode is activated and disturbances are expected. After switching to the boost mode, the upper threshold level is activated and the inverter keeps working in the boost mode. The input voltage continues declining until MPP is reached. In the example case, it is 320 V.

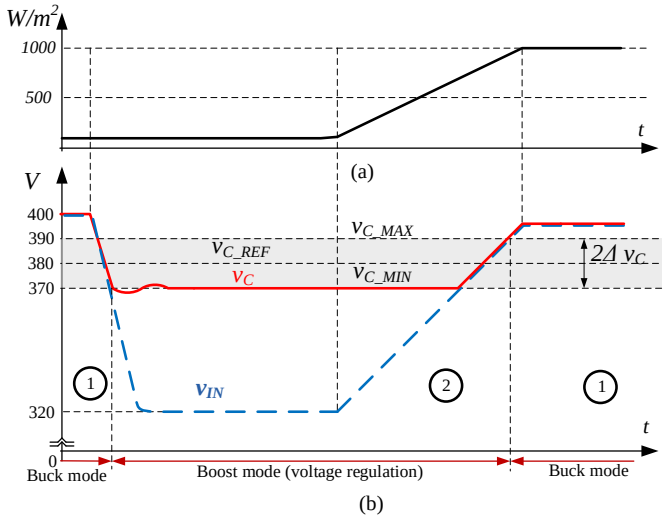

Fig. 4. Hysteresis band between the buck and boost modes during MPPT scanning: solar irradiation (a), capacitor voltage v_C and input voltage v_{IN} (b).

Further solar irradiation increase will lead to the MPPT voltage and capacitor voltage increase. In this case, the adoption of a voltage reference v^*_C voltage is required up to reaching the upper threshold level 390 V. After that, the buck mode will be activated and will remain stable despite some capacitor voltage oscillation. It is important to mention that the active state of the buck or boost voltage control mode is defined by a hysteresis band. The width of the hysteresis band $2\Delta v_C$ is defined by the empirical study and is addressed in the experimental section. Obviously, a wide band of hysteresis would result in more capacitor voltage floating in a long interval during the buck mode. The reference capacitor voltage that is the border between the buck and boost modes along with the hysteresis band can be considered as parameters for tuning and optimization of the converter performance.

Similar approach is also applied for GMPPT. After reaching lower threshold reference of the capacitor voltage, the boost mode is activated. As a result, the ST duty cycle (D_{ST}) value is increasing from 0 until its maximum value. Due to the noise and some oscillation across voltage, in order to avoid any trimming around buck-boost transient, the hysteresis band is required. Straight after boost mode activation, the voltage reference v_C* increased to 390 V. This approach provides a smooth and controllable transient from the buck to the boost mode during the GMPPT activation.

VI. MPPT AND GMPPT IMPLEMENTATION

This section describes the MPPT implementation for the buck and boost modes along with features of GMPPT implementation. Numerous papers are devoted to the different MPPT strategies for very general applications. From the research discussed above and own practical experience, it is concluded that the incremental conductance method with the output integrator may provide excellent MPPT performance considering dynamic and stability in the MPP [40]. Also, it is not sensitive to the slope of the PV curve.

Fig. 5 shows the sketch of the implemented MPPT technique. After data measurement and PLL calculation, the converter has an opportunity to select a GMPPT or MPPT scenario. The higher control level is in response to the selection between MPPT and GMPPT activation. There are many factors during the decision making but they are out of scope of this work. This work describes the realization of the MPPT and GMPPT approach.

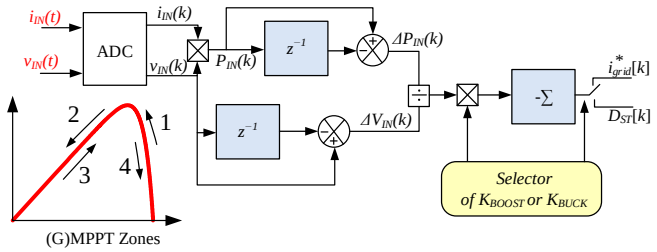

Fig. 5. Simplified sketch of the (G)MPPT.

In both cases, there is a difference between the buck and boost modes. In the buck mode, MPPT provides output reference current while in the boost case, ST duty cycle. Both methods have corresponding integrating coefficients K_{BOOST} and K_{BUCK}.

In the continuous and discrete time domains, the expression for the buck mode is the following:

$$I_{grid}{}^{*}(t) = -K_{BUCK}\int_0^t \frac{dP_{IN}}{dV_{IN}}(t)dt\,, \tag{5}$$

$$I_{grid}{}^{*}[k] = I_{grid}{}^{*}[k-1] - K_{BUCK}\frac{\Delta P_{IN}[k]}{\Delta V_{IN}[k]}\,. \tag{6}$$

The expression for the boost mode is similar:

$$D_{ST}(t) = -K_{BOOST}\int_0^t \frac{dP_{IN}}{dV_{IN}}(t)dt\,, \tag{7}$$

$$D_{ST}[k] = D_{ST}[k-1] - K_{BOOST}\frac{\Delta P_{IN}[k]}{\Delta V_{IN}[k]}\,. \tag{8}$$

These coefficients K_{BOOST} and K_{BUCK} along with variable N_{MPPT}, which defines the MPPT sampling frequency, are the objects of tuning. Trial and error method is the most effective method in this case. The MPPT sampling frequency was varying from 5 Hz up to 10 Hz. In order to derive a stable and high MPPT efficiency, different coefficients are required for different zones and operation points. It was the main object of tuning. For example, K_{BOOST} was $25\cdot10^{-6}$, while K_{BUCK} was varying from 0.1 to 0.5 in the continuous time domain. In order to apply these coefficients in the discrete form, they have to be divided by sampling frequency.

The main goal of the coefficient varieties approach consists in keeping precise and stable MPPT performance. In particular, if we are in the second zone, an increase of further reference power or ST states may lead to falling out of the working area. This, in turn, means that K_{BOOST} and K_{BUCK} coefficients have to be increased, while N_{MPPT} , which defines the sampling time,

has to be decreased in order to check the situation with the PV system sooner. Other zones are not critical in terms of stability, but tuning is required in order to achieve precise operation with minimal disturbances.

The GMPPT is also divided for buck and boost operation. The main goal of GMPPT scanning is to check the whole range of possible input voltage from the connected PV profile. As a result, the GMPPT algorithm is intended for permanent voltage decrease. Table II illustrates the difference between the MPPT and GMMPT implementation for the buck and boost modes. It contains signs of the K_{BOOST} and K_{BUCK} coefficients that have to be taken into account in Eqs. (2) and (4). In the case of MPPT, the main conclusion involves the modifications that can be done for the incremental conductance method with the output integrator in the buck mode. MPPT zones are shown in Fig. 5. The sign of the integrator in Zone 3 can be reversed. Zone 3 corresponds to the MPP approaching from the left side. In the boost mode, the input voltage is increasing and it corresponds to the ST duty cycle decreasing, while in the buck mode, the output signal of the integrator corresponds to the reference power.

TABLE II.
MPPT AND GMPPT IMPLEMENTATION

Zone	dP/dV	dV	MPPT Sampling frequency	MPPT (GMPPT)	
				Kbuck	Kboost
1	<0	<0	5	+(+)	+(+)
2	>0	<0	10	+(0)	+(0)
3	>0	>0	5	-(+)	+(0)
4	<0	>0	5	+(+)	+(+)

The difference between the MPPT and GMPPT modes is more significant. For example, in the case of MPPT operation, after reaching Zone 2 (input voltage and power were decreased), the K_{BUCK} and K_{BOOST} coefficients remain positive; according to Eq. (2), the reference power of the grid decreases and returns the MPP. Zone 3 is expected to be detected during the next step. This approach maintains power balance between the grid and the PV system around MPP. In the case of GMPPT algorithm, after detecting Zone 2, the K_{BUCK} and K_{BOOST} coefficients are equal to 0. It means that the same reference power or the ST duty cycle after MPP passing is maintained. The corresponding zero coefficients are shown in Table II. In this case, the power balance between the grid and the PV system will be disturbed, which, in turn, will lead to the voltage declining. If no other peak of the power is detected, this power will correspond to the global MPP. At the same time, it should be mentioned that after reaching the boost mode, the reference power can be decreased due to switching to the voltage controller across the capacitor (Fig. 2*b*), while the input voltage declining will be provided by the constant ST duty cycle.

The main goal of the GMPPT algorithm is to provide scanning of the whole input voltage range. Undesirable Zone 3 cannot be observed in GMPPT due to the action in Zone 2. Zone 3 can be detected in the GMPPT mode only due to the accuracy of the measurement system. If it happens, then it is recommended to keep K_{BOOST} equal to 0, while it is better to keep K_{BUCK} very small but negative. Positive K_{BUCK} in Zone 3 would lead to the reference current decreasing and as a result, to slowing down the MPPT performance. Zones 1 and 2 are mostly involved in the GMPPT mode that provides consistent input voltage declining. Despite the power, balance cannot be achieved in all operation points during GMPPT routine, it helps to define where the global MPP is located.

VII. EXPERIMENTAL VERIFICATION

The proposed approach was verified by a laboratory prototype of the system presented in Fig. 6. Component specifications were the same as in Table I. prototype can accept up to 3.3 kW input power. The best efficiency is expected around 2 kW input power. This power point is selected in order to maximize the Euro Efficiency.

Chroma 62150H-1000S power supply (PV simulator) was used for testing different PV profiles and operating points. Precision power analyzer YOKOGAWA WT1800 along with the digital oscilloscope Tektronix MDO4034B-3 were utilized for measurements. MOSFETs of type IPW65R041CFD are used as power switches. TLI4970 current sensors with digital output are used to measure current, while an ACPL-C87A isolation amplifier is applied for voltage sensing. The single-phase 230 V distribution system was emulated by one of the terminals available on a power auto-transformer. The PV simulator emulated the PV array. The control board based on DSP and FPGA is utilized. It allows to realize very flexible algorithms. Other parameters related to the experimental prototype are similar to those described in section II.

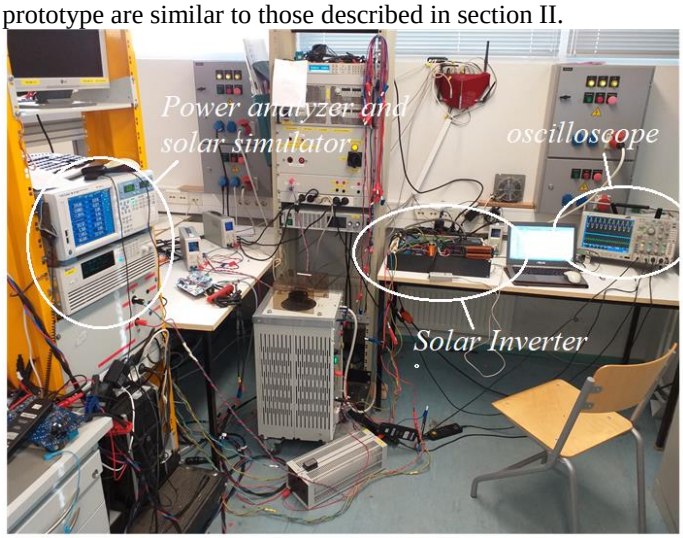

Fig. 6. A general view of the laboratory prototype of the solar inverter presented in Fig. 1.

To enable better analysis and discussion of the experimental results, a reference point $v_C^* = 380$ V, similar to that presented in (1), was considered during prototype evaluation. Table III shows considered PV profiles during the prototype evaluations presented and discussed. These profiles correspond to the Fig. 2*b*.

TABLE III.
PV ARRAY PROFILES CONSIDERED DURING EXPERIMENTAL EVALUATIONS

Profile	V_{oc}	V_{mpp}	I_{sc}	I_{mpp}	P_{mpp}
A	495 V	390 V	5.5 A	5.1 A	2.0 kW
B	400 V	320 V	5.5 A	5.1 A	1.6 kW
C	440 V	370 V	3.2 A	2.8 A	1.0 kW

First of all, a startup of the prototype system under the buck

control mode followed by the MPPT stable operation condition is presented in Fig. 7*a*. The PV array was adjusted with profile A. As can be noticed from the initial value of the voltage v_C, it corresponds to the open circuit voltage value from the PV array profile A. However, it is slightly larger than the output PV voltage v_{IN} due to the minor oscillation transient process during terminals connection and startup operation. After startup, the voltage v_C dropped down according to the buck mode of the proposed voltage control.

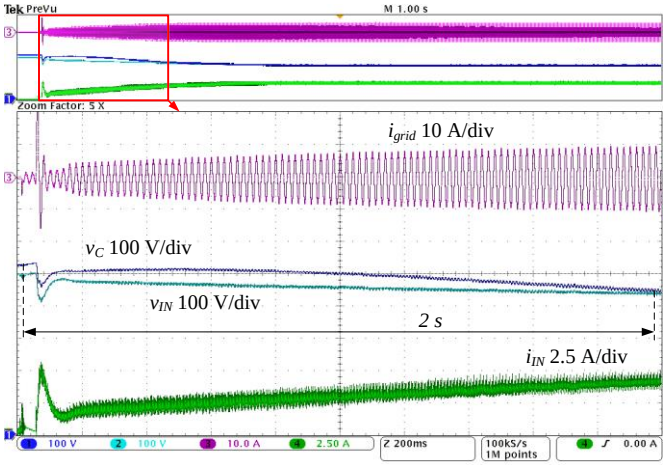

(a)

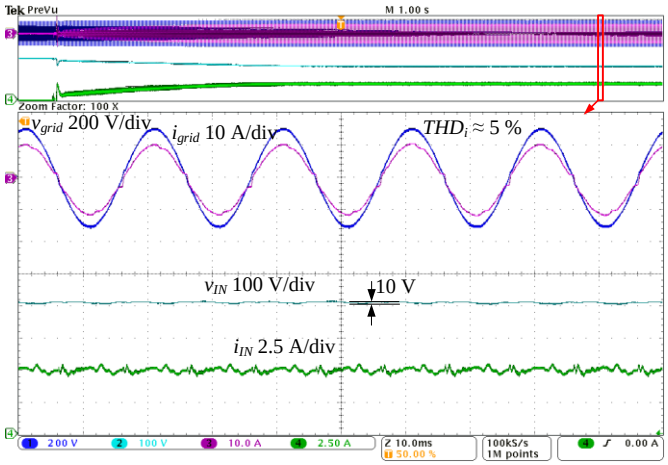

(b)

Fig. 7. System startup under the PV array profile A and the buck voltage control mode (a) along with zoomed diagram in steady-state mode (b).

It should be mentioned that the increase of the grid power reference was also defined by the MPPT algorithm; consequently, a smooth decrease of the voltage v_C was verified during the buck voltage control mode. Under those conditions, the average value of the voltage v_C only reflects the tendency of the input voltage v_{IN} according to (1) while the PV array can supply the grid power demand required by the MPPT algorithm.

It can be seen that MPP is reached in 2 seconds with the MPPT efficiency about 99 %, which corresponds to industrial standards. Additionally, Fig. 7*b* shows zoomed in picture the grid current, grid voltage, input current and input voltage. It can be seen that grid current has some oscillation, but not higher than 5 %. The PR controller was tuned to compensate 3rd, 5th, 7th and 9th harmonics in order to provide acceptable power quality.

In the second case, profile B was tested (Fig. 8). According to Fig. 8*a*, a decrease of the voltage v_{IN} after the system startup was also expected until the moment that the voltage v_C becomes lower than the minimum hysteresis level (370 V). Right after that, the proposed voltage control method was shifted to the boost control mode and the feedback regulation of the tuned $C_V(z)$ was able to achieve and hold a zero steady-state voltage error.

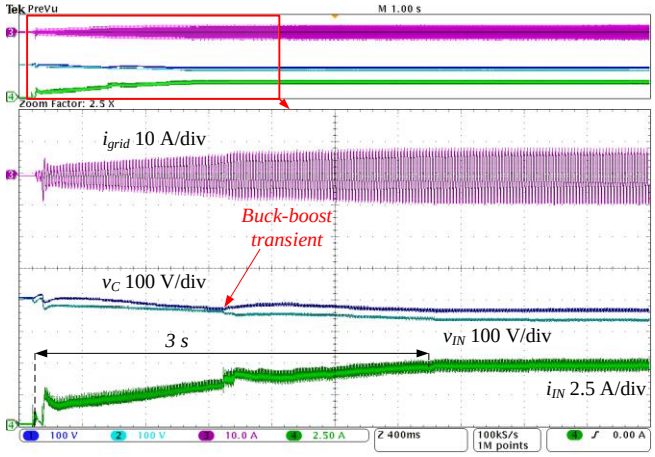

(a)

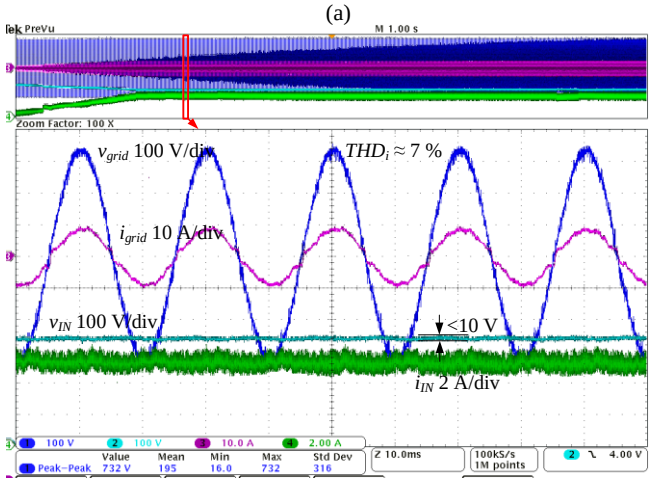

(b)

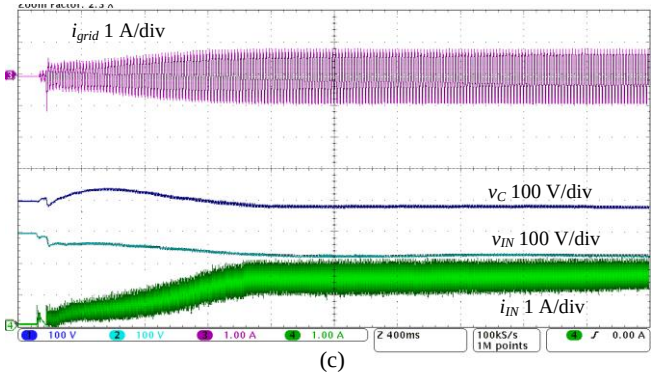

(c)

Fig. 8. System startup under the PV array profile B, which demonstrates shifting from buck to boost voltage control mode (*Vmpp* = 320 V) (a) along with zoomed diagram in steady-state mode (b) and low 300 W input power (c).

According to Fig. 2, the ST duty cycle corresponds to an

external perturbation signal in terms of the feedback control loop. For that reason, any external perturbation from the MPPT algorithm observed on v_C/v_{IN} and i_{grid}/i_{IN} relations was totally rejected by means of the tuned proposed discrete-time voltage controller.

Besides, high damping of grid power oscillations provided by the tuned $C_V(z)$, it also ensured a stable operation of the MPPT method around the global MPP (*320 V, 5.1 A*). Similar to the buck case, there was no significant oscillation in the capacitor voltage v_C, but a transient between the buck and boost mode can be noticed. MPP is reached in 3 seconds.

Fig. 8*b* shows the steady state mode of the converter. It can be seen that compared to the operation at 2 kW, the output current has more evident ripple but THD is not higher than the required 8%. Input voltage ripple is not higher than 3 %. In deference to profile A, this case has more evident high switching ripple in the input current. It is explained by ST utilization. But due to the low MPPT sampling frequency and averaged measurements between samples it does not have direct effect on the MPPT efficiency. Further power decreasing (solar radiation reduction) leads to the MPPT deterioration to 98 %. Fig. 8*c* shows extremely low input current and input voltage below 300 V (220 V MPP). In this case, the current ripple is increased but control is stable due to the switching frequency increasing. MPPT decreasing is unavoidable and explained by very flat PV curve in this case.

In order to underline the influence of the proposed hysteresis band during the transient between buck and boost control modes, an additional test was carried out. Fig. 9*a* and *b* show a similar test for Profile A but with lower solar irradiance.

In this case, the MPP is expected around 370 V, 2.8 A. The hysteresis band between the buck and boost modes is present (Fig. 9*a*) and MPP is reached in 4 seconds. The value of the hysteresis band is selected based on experimental tuning. From several experimental tests, we recommend to set the width of the hysteresis band slightly higher than low frequency voltage ripple across the internal capacitor. In our case it was ±10 V. It depends on the voltage ripple across the capacitors in the steady state mode and accuracy of the measurement system. In the second case (Fig. 9*b*), the hysteresis band is removed and some oscillations are observed. It is simply explained by the input voltage and capacitor voltage disturbances during the transient between the buck and boost modes. Also, the accuracy of the measurement system becomes extremely important. Any noise disturbance leads to the erroneous operation of the transition between the buck and boost modes.

It should be underlined that this was the worst case scenario observed and demonstrated. In most of the cases, some additional time delay can be observed in the algorithm performance that has no significant influence on the quality of the MPPT performance. In any case, the main conclusion is that the presence of the hysteresis improves the MPPT performance.

Finally, the GMPPT performance was tested in the partially shaded conditions of Profile A with several peaks. It is assumed that several panels are partially shaded, which results in 3 MPPs. The first one corresponds to the higher voltage and low current, which results in low power. The third scanned point has lower voltage but significantly higher current. The middle point has the highest power. According to the above described GMPPT approach, in order to scan the whole input voltage range, some time is needed. Fig. 10 shows the GMPPT routine.

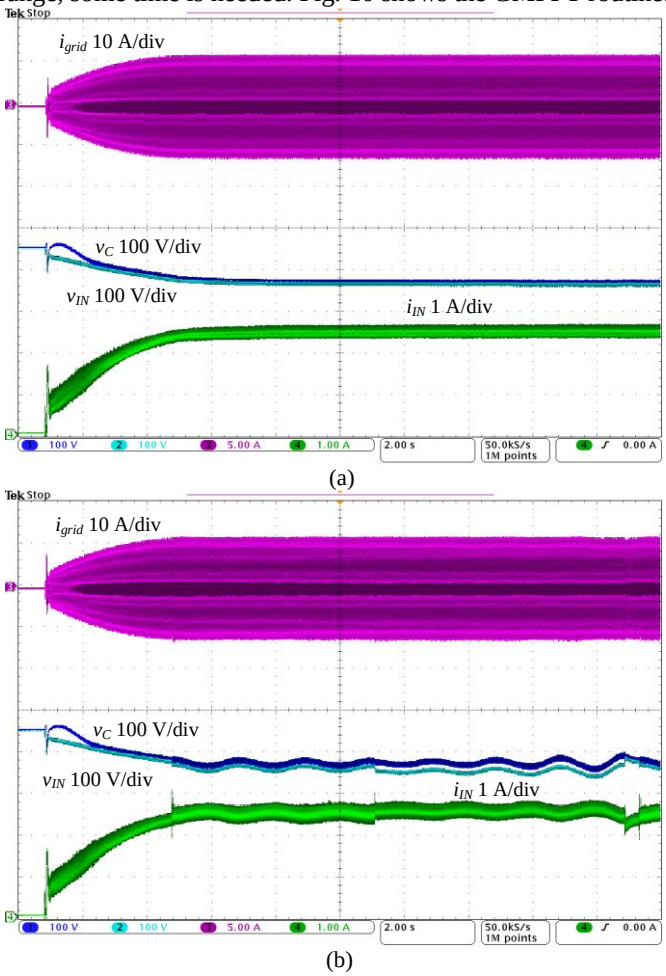

Fig. 9. MPPT performance demonstration with MPP in the border between buck and boost modes: with hysteresis band (a) and without (b).

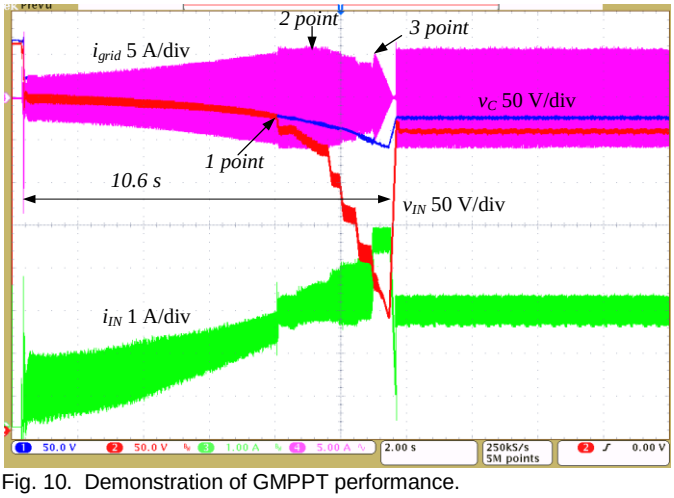

Fig. 10. Demonstration of GMPPT performance.

It can be seen that at the beginning, the solar inverter starts to inject power to the grid. The input voltage is declining from maximum to minimum level while the grid current has 3 obvious peaks that are caused by the partial shading. The scanning process finishes after 10.6 seconds. At the next

moment, the detected maximum power value during the GMPPT routine is set and stabilized by the local MPPT algorithm. It should be noted that obvious nonlinearity of the input voltage declining is observed. At the same time, it is not considered as a problem and is explained by the nonlinear ratio between the PV power and voltage. Finally, the GMPPT algorithm can be considered as an alternative solution to the conventional MPPT. Despite the longer operation time, it may have evident benefits if partial shading conditions are expected. In a very general case, the number of power peaks can be larger and the highest power value will be selected. Also, the speed of scanning of GMPPT can be increased by corresponding coefficients, but the accuracy can be lower.

VIII. Conclusions

This study proposed a novel MPPT and GMPPT scenario for the single-phase qZS-based grid-connected inverter with the buck-boost mode control. According to the dynamics of the PV systems, a wide range of the input dc voltage is expected. Based on our buck-boost control approach, which is the main outcome of this work, the following can be concluded:

1. To provide stable and efficient performance of the qZS-based inverter without ST utilization in the buck mode, different control strategies are recommended for the realization of the buck and boost mode.
2. To provide a smooth transient between two different control strategies, the hysteresis band was implemented.
3. IC method with variable sampling frequency and variable integral coefficients of the output integrator is recommended for MPPT and GMPPT realization.
4. It was shown that GMPPT, firstly implemented in the qZS-based inverter, requires 2-3 times longer period to find the global maximum, but can be an effective solution in partial shadow conditions.

All the statements were verified by the experimental evaluation. Different dc input voltage and power value levels were considered. MPPT efficiency was about 99% in the tested points and it requires 2-3 seconds to find a local maximum from the starting point. The proposed control approach is recommended for industrial implementation and can be applied in any Z-source or qZ-source-based inverter using relative values of the derived coefficients. Absolute values have to be tuned according to the particular parameters and passive components.

References

[1] F.Z. Peng, "Z-Source Inverter," *IEEE Trans. Ind. Appl., vol. 39*, no. 2, pp. 504-51, Mar/Apr. 2003.

[2] J. Anderson, F.Z. Peng, "Four quasi-Z-Source inverters," in *proc. of IEEE Power Electronics Specialists Conference (PESC'08)*, Jun. 2008, pp. 2743-2749.

[3] D. Vinnikov, I. Roasto, "Quasi-Z-Source-Based Isolated DC/DC Converters for Distributed Power Generation," *IEEE Trans. Ind. Electron.*, vol. 58, no. 1, pp. 192-201, Jan. 2011.

[4] N. S. González-Santini, H. Zeng, Y. Yu, F.Z. Peng "Z-Source Resonant Converter With Power Factor Correction for Wireless Power Transfer Applications" *IEEE Trans. on Power Electron.*, vol. 31, no. 11, pp. 7691 – 7700, Nov. 2016.

[5] D. Vinnikov, A. Chub, E. Liivik, R. Kosenko, O. Korkh, "Solar Optiverter—A Novel Hybrid Approach to the Photovoltaic Module Level Power Electronics", *IEEE Trans. Ind. Electron.*, vol. 66, no 5, pp. 3869 - 3880, May. 2018.

[6] S. Kouro, M. Malinowski, K Gopakumar, J. Pou, L.G Franquelo, B. Wu, J. Rodriguez, M.A. Perez, J.I. Leon, "Recent advances and industrial applications of multilevel converters," *IEEE Trans. Ind. Electron*., vol. 57, no.8, pp.2553-2580, Aug. 2010.

[7] Y. Liu, G. Baoming, H. Abu-Rub, F.Z. Peng, "An Effective Control Method for Quasi-Z-Source Cascade Multilevel Inverter-Based Grid-Tie Single-Phase Photovoltaic Power System", *IEEE Trans. Ind. Informatics*, vol. 10, no 1, pp. 399-407, Feb. 2014.

[8] O. Husev, C. Roncero-Clemente, E. Romero-Cadaval, D. Vinnikov, S. Stepenko, "Single phase three-level neutral-point-clamped quasi-Z-source inverter", *IET Power Electron.*, vol. 8, no. 1, pp. 1-10, Jan. 2015.

[9] S. Bayhan, P. Kakosimos, H. Abu-Rub, J. Rodriguez, "Model predictive control of five-level H-bridge neutral-point-clamped qZS inverter," in *Proc. of IECON 2016 - 42nd Annual Conference of the IEEE Industrial Electronics Society*.

[10] B. Ge, Y. Liu, H. Abu-Rub, F. Z. Peng, "State-of-Charge Balancing Control for Battery Energy Stored Quasi-Z Source Cascaded Multilevel Inverter Based Photovoltaic Power System". *IEEE Trans. on Ind. Electron.*, vol. 65, no.3, pp. 2268-2279, Aug. 2018.

[11] R. Burkart, J.W. Kolar, G. Griepentrog, "Comprehensive comparative evaluation of single- and multi-stage three-phase power converters for photovoltaic applications," in *Proc. of Intelec, 2012*, pp. 1-8.

[12] D. Panfilov, O. Husev, F. Blaabjerg, J. Zakis, K. Khandakji, "Comparison of three-phase three-level voltage source inverter with intermediate dc-dc boost converter and quasi-Z-source inverter", *IET Power Electron.*, vol. 9, no. 6, pp. 1238-1248, May. 2016.

[13] O. Husev, D. Vinnikov, C. Roncero-Clemente, A. Chub, E. Romero-Cadaval, "Single-Phase String Solar qZS-based Inverter: Example of Multi-Objective Optimization Design." *IEEE Trans. on Ind. Appl.*, vol. 57, no.3, pp. 3120 - 3130, May-June 2021.

[14] E. Kabalci, "The Design and Analysis of a Two-Stage PV Converter with Quasi-Z Source Inverter," in *proc. of IEEE 18th International Power Electronics and Motion Control Conference (PEMC)*, 2018.

[15] Y. Zhou, Hongbo Li, Hui Li, "A Single-Phase PV Quasi-Z-Source Inverter With Reduced Capacitance Using Modified Modulation and Double-Frequency Ripple Suppression Control". *IEEE Trans. Power Electron.*, vol. 31, no.3, pp. 2166-2173, Mar. 2016.

[16] J.-H. Park, H.-G. Kim, E.-C. Nho, T.-W. Chun, "Capacitor voltage control for MPPT range expansion and efficiency improvement of grid-connected Quasi Z-Source Inverter", in *the proc. of The 2010 International Power Electronics Conference - ECCE ASIA*.

[17] M. Uno, T. Shinohara, "Module-Integrated Converter Based on Cascaded Quasi-Z-Source Inverter With Differential Power Processing Capability for Photovoltaic Panels Under Partial Shading", *IEEE Trans. Power Electron.*, vol. 34, no.12, pp. 11553 - 11565, Dec. 2019.

[18] L. Yushan, H. Abu-Rub, G. Baoming, P. FangZheng, A. T. de Almeida, and F.J.T.E. Ferreira, "An improved MPPT method for quasi-Z-source inverter based grid-connected photovoltaic power system," in *the proc. of ISI*, 2012, pp. 1754-1758.

[19] S. Ahmadzadeh, G.A. Markadeh, "Incremental conductance based MPPT using a high step-up Y-source DC-DC Converter", in *proc. of 8th Power Electronics, Drive Systems & Technologies Conference (PEDSTC)*, 2017.

[20] D. Vinnikov, A. Chub, O. Korkh, E. Liivik, F. Blaabjerg, S. Kouro, "MPPT performance enhancement of low-cost PV microconverters," *Solar Energy*, vol. 187, no. 15, pp. 156-166, Jul. 2019.

[21] M. Metry, Y. Liu, R.S. Balog, H. Abu-Rub, "Model predictive control for maximum power point tracking of quasi-Z-source inverter based grid-tied photovoltaic power system," in *the proc. of Industrial Electronics (ISIE), 2017 IEEE International Symposium on*, 2017, pp. 1657-1662.

[22] M. Nikroo, S.H. Montazeri, J. Milimonfared, F. Shadian, "Performance Analysis of Model Predictive Controller for Grid-Connected Quasi Z-Source and Split-Source PV Inverters", *in proc. of 11th Power Electronics, Drive Systems, and Technologies Conference*, 2020.

[23] S. Sajadian, R. Ahmadi, H. Zargarzadeh, "Extremum Seeking-Based Model Predictive MPPT for Grid-Tied Z-Source Inverter for Photovoltaic Systems," *IEEE Journal of Emerging and Selected Topics in Power Electronics*, vol. 7, no. 1, pp. 216-227, Aug. 2020.

[24] A. Mohapatra, B. Nayak, P. Das, K. Barada Mohanty, "A review on MPPT techniques of PV system under partial shading condition," *Journal of Renewable and Sustainable Energy Reviews*, vol. 80, pp. 854-867, Dec. 2017.

[25] J. Gosumbonggot, Duy-Dinh Nguyen, G. Fujita, "Partial Shading and Global Maximum Power Point Detections Enhancing MPPT for Photovoltaic Systems Operated in Shading Condition" *in proc. of 2018 53rd International Universities Power Engineering Conference (UPEC).*

[26] Al-Wesabi Ibrahim, M.B. Shafik, M. Ding, M. Abu Sarhan, Z. Fang, A.G. Alareqi, T. Almoqri, A.M. Al-Rassas, "PV maximum power-point tracking using modified particle swarm optimization under partial shading conditions", *Chinese Journal of Electrical Engineering*, pp. Vol. 6, no. 4, pp. 106 – 121, Dec. 2020.

[27] S. B. Santra, D. Chatterjee, K. Kumar, M. Bertoluzzo, A. Sangwongwanich, F. Blaabjerg, "Capacitor Selection Method in PV Interfaced Converter Suitable for Maximum Power Point Tracking," *IEEE Journal of Emerging and Selected Topics in Power Electronics*, vol. 9, no. 2, pp. 2136-2146, Apr. 2021.

[28] M. Liserre, F. Blaabjerg, and S. Hansen, "Design and Control of an *LCL*-Filter-Based Three-Phase Active Rectifier," *IEEE Trans. Ind. Appl.*, vol. 41, no. 5, pp. 1281-1291, Sep/Oct. 2005.

[29] H. Hu, S. Harb, N. Kutkut, I. Batarseh, Z. Shen, "A review of power decoupling techniques for micro-inverters with three different decoupling capacitor locations in PV systems," *IEEE Trans. Power Electron.*, vol. 28, no. 6, pp. 2711–2726, Jun. 2012.

[30] Y. Tang, F. Blaabjerg, "Power decoupling techniques for single-phase power electronics systems — An overview," in *proc. of IEEE Energy Conversion Congress and Exposition (ECCE)*, 2015.

[31] C. R. Sullivan, J. Awerbuch, A. M. Latham, "Decrease in photovoltaic power output from ripple: Simple general calculation and effect of partial shading", in *proc. of Twenty-Sixth Annual IEEE Applied Power Electronics Conference and Exposition (APEC)*, 2011.

[32] S. P. Pimentel, O. Husev, D. Vinnikov, C. Roncero-Clemente, E. Makovenko, and S. Stepenko, "Voltage control tuning of a single-phase grid-connected 3L qZS-based inverter for PV application," in *proc. of 2018 IEEE 38th International Conference on Electronics and Nanotechnology (ELNANO 2018)*, Kiev, 2018.

[33] Y. Li, S. Jiang, J. G. Cintron-Rivera and F. Z. Peng, "Modeling and Control of Quasi-Z-Source Inverter for Distributed Generation Applications," *IEEE Trans. on Ind. Electron.*, vol. 60, no. 4, pp. 1532-1541, Apr. 2013.

[34] O. Husev, C. Roncero-Clemente, E. Makovenko, S. Pires Pimentel, D. Vinnikov, J. Martins, "Optimization and Implementation of the Proportional-Resonant Controller for Grid-Connected Inverter with Significant Computation Delay," *IEEE Trans. on Ind. Electron*, vol. 67, no 2, pp. 1201 - 1211, Feb. 2020.

[35] Jong-Kyu Kim, Jong-Hyun Lee, Hea-Gwang Jeong, and Kyo-Beum Lee, "Improvement of Grid-Connected Inverter Systems with PR Controllers under the Unbalanced and Distorted Grid Voltage", in *proc. of 2012 IEEE 7th International Power Electronics and Motion Control Conference - ECCE* Asia June 2-5, 2012, Harbin, China.

[36] C. Roncero-Clemente, E. Romero-Cadaval, M. Ruiz-Cortés, O. Husev, "Carrier Level-Shifted Based Control Method for the PWM 3L-T-Type qZS Inverter With Capacitor Imbalance Compensation," *IEEE Trans. Ind. Electron.*, vol. 65, no. 5, pp. 4820 - 4830, May. 2019.

[37] T. Shults, O. Husev, C. Roncero-Clemente, F. Blaabjerg, R. Strzelecki, "Design of three-phase three-level CIC T-source inverter with maximum boost control", *in proc. of IECON 2015-41st Annual Conference of the IEEE Industrial Electronics Society*.

[38] T. Shults, O. Husev, F. Blaabjerg, C. Roncero, E. Romero-Cadaval, D. Vinnikov. "Novel Space Vector Pulse Width Modulation Strategies for Single-Phase Three-Level NPC Impedance-Source Inverters," *IEEE Trans. Power Electron*, Vol. 34, No. 5, pp. 1281-1291, Sep/Oct. 2005.

[39] Y. Liu, B. Ge, H. Abu-Rub, F. Z. Peng, "An Effective Control Method for Quasi-Z-Source Cascade Multilevel Inverter-Based Grid-Tie Single-Phase Photovoltaic Power System," *IEEE Trans. on Ind. Informatics*, vol. 10, no 1, pp. 399 - 407, Feb. 2014.

[40] M. A. G. de Brito, L. Galotto, L. P. Sampaio, G. A. Melo and C. A. Canesin, "Evaluation of the main mppt techniques for photovoltaic applications," *IEEE Trans. on Ind. Electron.*, vol. 60, no. 3, pp. 1156-1167, Mar. 2013.

Oleksandr Husev (S'10–M'12-SM'19) received the B.Sc. and M.Sc. degrees in industrial electronics from Chernihiv State Technological University, Chernihiv, Ukraine, in 2007 and 2008 respectively. He defended PhD thesis in the Institute of Electrodynamics of the National Academy of Science of Ukraine in 2012.
He is senior researcher and project leader of the Department of Electrical Power Engineering and Mechatronics, TalTech University He has over 100 publications and is the holder of several patents.
His research interests are in Power Electronics systems. Design of novel topologies, control systems based on a wide range of algorithms, including modeling, design, and simulation. Applied design of power converters and control systems and application, stability investigation.

Dmitri Vinnikov (IEEE M'07, SM'11) received the Dipl. Eng., M.Sc., and Dr. Sc. techn. degrees in electrical engineering from Tallinn University of Technology, Tallinn, Estonia, in 1999, 2001, and 2005, respectively. He is currently the Head of the Power Electronics Group, Department of Electrical Power Engineering and Mechatronics, Tallinn University of Technology (Estonia). He is the Head of R&D and co-founder of Ubik Solutions LLC - Estonian start-up company dedicated to innovative & smart power electronics for renewable energy systems. Moreover, he is one of the founders and leading researchers of ZEBE – Estonian Centre of Excellence for zero energy and resource efficient smart buildings and districts. He has authored or coauthored two books, five monographs and one book chapter as well as more than 300 published papers on power converter design and development and is the holder of numerous patents and utility models in this field. His research interests include applied design of power electronic converters and control systems, renewable energy conversion systems (photovoltaic and wind), impedance-source power converters, and implementation of wide bandgap power semiconductors. D. Vinnikov is a Chair of the IEEE Estonia Section.

Carlos Roncero-Clemente received the international Ph.D. degree in electrical, electronic and control engineering from the University of Extremadura (Spain) in 2016. During his Ph.D. research, he was a visiting student with the Tallinn University of Technology and Aalborg University. He was a postdoctoral researcher with the Nova University of Lisbon (2016-2019). He is currently a senior researcher in power electronic and renewable energies with the University of Extremadura. His research interests include power electronic topologies and controls for renewable energy applications and smart grids. He is author of more than 30 journal papers and 75 international conferences.

Frede Blaabjerg (S'86–M'88–SM'97–F'03) was with ABB-Scandia, Randers, Denmark, from 1987 to 1988. From 1988 to 1992, he got the PhD degree in Electrical Engineering at Aalborg University in 1995. He became an Assistant Professor in 1992, an Associate Professor in 1996, and a Full Professor of power electronics and drives in 1998. From 2017 he became a Villum Investigator. He is honoris causa at University Politehnica Timisoara (UPT), Romania and Tallinn Technical University (TTU) in Estonia.

His current research interests include power electronics and its applications such as in wind turbines, PV systems, reliability, harmonics and adjustable speed drives. He has published more than 600 journal papers in the fields of power electronics and its applications. He is the co-author of four monographs and editor of ten books in power electronics and its applications.

He has received 33 IEEE Prize Paper Awards, the IEEE PELS Distinguished Service Award in 2009, the EPE-PEMC Council Award in 2010, the IEEE William E. Newell Power Electronics Award 2014, the Villum Kann Rasmussen Research Award 2014, the Global Energy Prize in 2019 and the 2020 IEEE Edison Medal. He was the Editor-in-Chief of the IEEE Transactions On Power Electronics from 2006 to 2012. He has been Distinguished Lecturer for the IEEE Power Electronics Society from 2005 to 2007 and for the IEEE Industry Applications Society from 2010 to 2011 as well as 2017 to 2018. In 2019-2020 he served as a President of IEEE Power Electronics Society. He has been Vice-President of the Danish Academy of Technical Sciences.

He is nominated in 2014-2020 by Thomson Reuters to be between the most 250 cited researchers in Engineering in the world.

Ryszard Strzelecki (born 1955, SM IEEE) graduated in industrial electronics from the Kyiv University of Technology, in 1981. He received the Ph.D. degree, in 1984, and the Habilitation (D.Sc.) degree in the theme prediction control of the self-commutation power electronics converters from the Institute of Electrodynamics, Academy of Sciences, Ukrainian Soviet Socialist Republic, Kiev, in 1991. In 1999, he received the title of Professor of technical sciences. He is currently a Full Professor with the Gdansk University of Technology, Poland, and a scientific consultant of the AREX Ltd (WB Group). He is the author of more scientific articles, monographs and patents. His interests focus on topologies, control methods and unconventional applications of power electronic systems.